

# Meridional Asymmetries in Forced Beta-Plane Turbulence

Iordanka N. Panayotova

*Old Dominion University, Department of Mathematics and Statistics, Norfolk, United States*

*E-mail: IPanayot@odu.edu*

*Received March 10, 2011; revised April 18, 2011; accepted June 4, 2011*

## Abstract

Forced geostrophic turbulence on the surface of a rotating sphere (so called  $\beta$ -plane turbulence) is simulated through the use of the  $\beta$ - $sQG^{+1}$  numerical model. Domain occupied by the fluid has a channel geometry with 512 by 256 grid points, periodic boundary conditions in x-direction and rigid boundaries in y-direction. Random forcing is applied at high wave-numbers in the spectral space. To better understand eddies dynamics we simulate both regimes, with and without stochastic forcing, starting from identical initial conditions. Direct numerical simulations exhibit different dynamical properties in different regimes. In the freely evolving case, a wave term that competes with inertia on large-scales (added as a result of the  $\beta$ -effect) produces high meridional asymmetries in the eddies spatial and time scales. This asymmetry is added to the standard for the  $\beta$ -plane turbulence zonal asymmetry. In the forced regime there is not only anisotropy in the eddies deformation radius, but also in their orientation. The preferred direction for the warm anomalies elongation is north-western, while for the cold anomalies is north-eastern. These results may explain the observed meridional meandering of the mid-latitude zonal jets.

**Keywords:** Beta-Plane Turbulence, Stochastic Forcing, Meridional Asymmetries

## 1. Introduction

Geostrophic turbulence is a chaotic three-dimensional nonlinear motion of the fluids that are near to the state of geostrophic and hydrostatic balance. The simplest three-dimensional model of the tropopause dynamics is a model with introduced a quasi-horizontal interface separating regions of homogeneous potential vorticity of differing values [1]. The quasi-geostrophic ( $QG$ ) approximation to this model (and the constant potential vorticity in the interior) reduces dynamics of the flow to quasi-two-dimensional turbulence. In this way, the three-dimensional flow is entirely modeled by the horizontal advection of potential temperature on the interface. This approximation is known as surface quasi-geostrophy ( $sQG$ ) [2].

The quasi-geostrophic theory and its numerical models have remained of interest to meteorologists and oceanographers for long time because they captured a number of physically important flow features while possessing a structure amenable to mathematical analysis and extensive numerical experimentations. However quasi-geostrophic approximation has one serious deficiency - its pervasive symmetry, and as a result it fails to explain a number of observed asymmetries in the large-scale phe-

nomena well known from observational studies.

From mathematical prospective the  $sQG$  model is a linear model. It can be obtained as the leading order approximation in an asymptotic expansion in small Rossby number. Rossby number ( $\varepsilon = U/fL$ ) is a dimensionless parameter obtained as the ratio between the characteristic velocity and the product of the length scale and Coriolis frequency. A small Rossby number characterizes a flow that is strongly affected by Coriolis forces. One way to reduce deficiencies of any linear model is to extend it with the nonlinear terms. Such a weakly nonlinear model was developed in [3] on an  $f$ -plane, *i.e.* the rotating fluid was approximated on a surface of rotating sphere with constant Coriolis parameter. The obtained model is known as  $f-sQG^{+1}$  model. In this way some additional 3D factors as ageostrophic advection, stretching, and tilting of relative vorticity were brought to the 2D flow dynamics. The model was able to capture some structural differences between cyclonic and anti-cyclonic vortices on the tropopause [3].

It is well known that the meridional variation in the Coriolis parameter (so called  $\beta$ -effect) has a prominent role in the large-scale dynamics producing Rossby waves and zonal jets [4]. Adding the  $\beta$ -effect into the weakly

non-linear dynamics of the extended Eady model [6] resulted in symmetry breaking and producing an arching wave-train as a neutral mode at finite amplitude. Including the  $\beta$ -effect in the nonlinear  $sQG^{+1}$  dynamics resulted in the so called  $\beta$ - $sQG^{+1}$  model [5] and produced high meridional asymmetry in the eddies spatial and time scales. That asymmetry was added to the standard for the  $sQG$   $\beta$ -plane turbulence zonal asymmetry [4].

This paper is focused on the numerical simulations of  $\beta$ - $sQG^{+1}$  model in the forced regime. To better understand the properties of the forced  $\beta$ -plane turbulence we run numerical simulations in two regimes, with and without stochastic forcing. Adding a random forcing to the model produced some novel meridional asymmetries as asymmetries in deformation radius and orientation of the coherent structure formations. The forcing term was applied in the spectral space and localized in the vicinity of large wave number  $k_f$ . For computational purposes a dissipation operator combining frictional and viscous terms was added to the system.

The rest of the paper is organized as follows. In section 2 we outline the  $\beta$ - $sQG^{+1}$  numerical model. Numerical simulations are described in section 3, and conclusions are discussed in section 4.

## 2. Numerical Model

For our numerical simulations we are interested in balanced motions of an adiabatic, inviscid, Boussinesq and hydrostatic rotating flow approximated on a mid-latitude  $\beta$ -plane channel. Such an approximation of the governing equations takes into account the meridional variation in the Coriolis parameter ( $f = f_0 + \beta y$ ). Balanced dynamics then is represented by the material conservation of Ertel potential vorticity (PV)  $q$  in the interior

$$\frac{Dq}{Dt} = \mathcal{D}q, \quad z > 0, \quad (1)$$

and potential temperature  $\theta$  on the rigid boundary

$$\frac{D\theta^s}{Dt} = \mathcal{D}\theta^s, \quad z = 0. \quad (2)$$

The perturbation potential vorticity is defined in terms of the primitive variables  $(u, v, \theta)$  by

$$q \equiv (v_x - u_y + \theta_z + \beta y) + \varepsilon [\beta y \theta_z - v_z \theta_x + u_z \theta_y + (v_x - u_y) \theta_z], \quad (3)$$

where  $\beta$  is the meridional variation in the Coriolis parameter  $f = 1 + \varepsilon \beta y$ , ( $\beta = \mathcal{O}(1)$ ) and  $\varepsilon = U/fL$  is the Rossby number ( $U$  is the characteristic velocity,  $L$

is the characteristic length). The operator  $\mathcal{D}$  is a dissipation operator defined by

$$\mathcal{D} = -\nu \nabla_H^8, \quad \nabla_H^2 = \partial_{xx} + \partial_{yy}. \quad (4)$$

Here we use an artificial hyper viscosity which is standard in the direct numerical simulations of turbulence, as it prevents the accumulation of energy at the smallest scales.

The material derivative is given by

$$\frac{D}{Dt} \equiv \frac{\partial}{\partial t} + u \frac{\partial}{\partial x} + v \frac{\partial}{\partial y} + \varepsilon w \frac{\partial}{\partial z}, \quad (5)$$

where  $\varepsilon$  is the Rossby number and  $(u, v, w)$  is the wind vector.

The channel model requires an additional boundary condition of no meridional flow through the channel walls

$$v = \Phi_x - G_z = 0, \quad y = \pm \pi/2l. \quad (6)$$

Assuming homogeneous potential vorticity  $q = \text{const}$  Equation (1) will be exact, so the balanced dynamics reduces to (2), *i.e.* to the horizontal advection of the surface potential temperature

$$\frac{\partial \theta^s}{\partial t} = -u^s \frac{\partial \theta^s}{\partial x} - v^s \frac{\partial \theta^s}{\partial y} + \mathcal{D}\theta^s. \quad (7)$$

The numerical solution now is obtained in two steps, potential temperature inversion and horizontal advection. First, horizontal winds  $(u, v)$  are recovered from the potential temperature  $\theta^s$  as solutions of the three-dimensional Poisson equations using an inversion process described in the next section. Then those approximate winds are used to advect  $\theta^s$  in (7).

### 2.1. Potential Temperature Inversions

For the potential temperature inversions we use small Rossby number expansions of all primitive variables. First we begin with the leading order (linear) equations, then we continue with the second order (nonlinear corrections) equations.

### 2.2. Leading Order Inversion

The leading order balance condition yields a standard quasi-geostrophic potential vorticity inversion for the leading order geopotential  $\Phi^{(0)}$ :

$$\nabla^2 \Phi^{(0)} = -\beta y, \quad z > 0; \quad (8)$$

$$\Phi_z^{(0)} = \theta^s, \quad z = 0.$$

Here the initial surface potential temperature is considered random. Dividing the leading order solution into

a zonal basic state component  $\bar{\Phi}$  and a disturbance part  $\Phi^e$ ,  $\Phi^{(0)} = \bar{\Phi} + \Phi^e$ , we get that

$$\bar{\Phi} = -\left(\bar{u}_0 + \Lambda z + \frac{\beta z^2}{2}\right)y. \quad (9)$$

The disturbance is the solution of the homogeneous equation

$$\Phi_{xx}^e + \Phi_{yy}^e + \Phi_{zz}^e = 0$$

that is decaying in the upward direction ( $\Phi^e = 0, z \rightarrow \infty$ ), with random initial conditions ( $\Phi_z^e = \theta^s, z = 0$ ), and vanishing on the vertical channel walls ( $\Phi^e = 0$ , on  $y = \pm\pi/(2l)$ ). Applying Fourier transform in zonal direction to this equation, and sine transform in meridional, we get the solution in the spectral space

$$\hat{\Phi}^e(k, l) = -\frac{\hat{\theta}^s(k, l)}{m} e^{-mz}. \quad (10)$$

Here hats denote spectral variables,  $k$  and  $l$  are  $x$  and  $y$  wave numbers, and  $m = \sqrt{k^2 + l^2}$ . The properties of sine transform guarantee that the boundary conditions on the vertical channel walls are satisfied.

Then the leading-order ( $QG$ ) winds are determined by applying first the inverse sine and then the inverse Fourier transform to the spectral winds, *i.e.*

$$(\hat{u}^0, \hat{v}^0) = (-il\hat{\Phi}^0, ik\hat{\Phi}^0).$$

### 2.3. First Order Inversion

Next-order corrections to the  $QG$  approximation are obtained by solving the three-dimensional Poisson equations, subject to the appropriate boundary conditions:

$$\nabla^2 F^{(1)} = 2J(\Phi_z^{(0)}, \Phi_x^{(0)}) - \beta y \Phi_{yz}^{(0)}, F^{1s} = 0; \quad (11)$$

$$\nabla^2 G^{(1)} = 2J(\Phi_z^{(0)}, \Phi_y^{(0)}) + \beta y \Phi_{xz}^{(0)}, G^{1s} = 0; \quad (12)$$

$$\nabla^2 \Phi^{(1)} = q^{(1)} - \left[ \left( \bar{\nabla}^2 \Phi^{(0)} \right) \Phi_{zz}^{(0)} - \left| \bar{\nabla} \Phi_z^{(0)} \right|^2 + \beta y \Phi_{zz}^{(0)} \right], \quad (13)$$

$$\Phi_z^{1s} = 0;$$

where  $\nabla^2 = \partial_{xx} + \partial_{yy} + \partial_{zz}$ .

To satisfy (6) we additionally require that for both  $G^{(1)}$  and  $\Phi^{(1)}$

$$G^{(1)} = 0 \quad \text{and} \quad \Phi^{(1)} = 0 \quad \text{on} \quad y = \pm\pi/(2l). \quad (14)$$

To find the first order nonlinear solutions to (11), (12), and (13) we use the fact that the right-hand sides of the inhomogeneous equations involve only the leading order solution  $\Phi^{(0)}$  so we can express the particular solutions to the Poisson equations as follows

$$F^{(1)} = \Phi_z^e \Phi_y^e - \frac{\left( \Lambda z + \frac{\beta z^2}{2} \right)}{m} \Phi_{xx}^e - \frac{\beta z}{2m^2} \Phi_{xx}^e - \frac{\beta y z}{2} \Phi_y^e - \frac{\beta z^2}{4m} \Phi_{yy}^e - \frac{\beta z}{4m^2} \Phi_{yy}^e + \frac{\beta y z^2}{2} \left( \Lambda + \frac{\beta z}{3} \right) - \frac{\Lambda \beta y z}{m}, \quad (15)$$

$$G^{(1)} = -\Phi_x^e \Phi_z^e - \frac{\left( \Lambda z + \frac{\beta z^2}{2} \right)}{m} \Phi_{xy}^e - \frac{\beta z}{4m^2} \Phi_{xy}^e + \frac{\beta y z}{2} \Phi_x^e + \frac{\beta z^2}{4m} \Phi_{xy}^e, \quad (16)$$

$$\Phi^{(1)} = \frac{(\Phi_z^e)^2}{2} - \beta y z \Phi_z^e - \Lambda z \Phi_y^e + \bar{\Phi}^{(1)}, \quad (17)$$

$$\bar{\Phi}^{(1)} = \frac{\beta^2 y^2 z^2}{2} + \frac{\beta \Lambda z^3}{6}.$$

Our goal is to find the **surface** winds, so from now on we can focus only on the surface potential vorticity inversion ( $z = 0$ ). Using the particular solutions (15), (16) and (17), we can specify the potentials on the surface ( $z = 0$ )

$$F^{(1)} = \Phi_y^e \Phi_z^e + \tilde{F}^{(1)}; G^{(1)} = -\Phi_x^e \Phi_z^e + \tilde{G}^{(1)}; \quad (18)$$

$$\Phi^{(1)} = \frac{(\Phi_z^e)^2}{2} + \tilde{\Phi}^{(1)}$$

The homogenous terms ( $\tilde{F}^{(1)}, \tilde{G}^{(1)}, \tilde{\Phi}^{(1)}$ ) satisfy the Laplace problems with corresponding boundary conditions, that allow ( $\tilde{F}^{(1)}, \tilde{G}^{(1)}, \tilde{\Phi}^{(1)}$ ) to satisfy (11), (12), (13), and (14)

$$\nabla^2 \tilde{F}^{(1)} = 0, \tilde{F}^{1s} = -\Phi_z^e \Phi_y^e; \quad (19)$$

$$\nabla^2 \tilde{G}^{(1)} = 0, \tilde{G}^{1s} = -\Phi_x^e \Phi_z^e; \tilde{G}^{(1)} = 0 \quad \text{on} \quad y = \pm\pi/(2l);$$

$$\nabla^2 \tilde{\Phi}^{(1)} = 0, \tilde{\Phi}^{1s} = -\Phi_z^e \Phi_{zz}^e + \beta y \Phi_z^e + \Lambda \Phi_y^e;$$

$$\tilde{\Phi}^{(1)} = 0 \quad \text{on} \quad y = \pm\pi/(2l).$$

Here superscript  $s$  denotes a surface value (on  $z = 0$ ). The condition of no normal flow through the vertical walls of the considered  $\beta$ -plane mid-latitude channel necessitates applying a sine transform in the meridional direction. A Fourier transform is applied in zonal direction. As a result, we can express derivatives of the next order potentials necessary for the surface winds

$$F_z^{(1)} = \left( \Phi_y^e \Phi_z^e \right)_z - \mathcal{F}^{-1} \left\{ -m \mathcal{F} \left[ \Phi_y^e \Phi_z^e \right] \right\}, \quad (20)$$

$$G_z^{(1)} = -\left( \Phi_x^e \Phi_z^e \right)_z + \mathcal{F}^{-1} \left\{ -m \mathcal{F} \left[ \Phi_x^e \Phi_z^e \right] \right\}, \quad (21)$$

$$\Phi_x^{(1)} = \Phi_{xz}^e \Phi_z^e + \mathcal{F}^{-1} \left\{ \frac{-ik}{m} \mathcal{F} \left[ -\Phi_z^e \Phi_{zz}^e + \beta y \Phi_z^e + \Lambda \Phi_y^e \right] \right\}, \quad (22)$$

$$\Phi_y^{(1)} = \Phi_{yz}^e \Phi_z^e + \mathcal{F}^{-1} \left\{ \frac{-il}{m} \mathcal{F} \left[ -\Phi_z^e \Phi_{zz}^e + \beta y \Phi_z^e + \Lambda \Phi_y^e \right] \right\}, \quad (23)$$

where  $\mathcal{F}$  means applying consequently the Fourier and sine transforms, respectively in the  $x$ - and  $y$ -directions, while  $\mathcal{F}^{-1}$  indicates the inverse of this process.

Then the horizontal winds can be approximated by these potentials with the order  $\mathcal{O}(\varepsilon^2)$

$$u^s \sim u^{s0} + \varepsilon u^{s1} = -\left( \Phi_y^{(0)} + \varepsilon \left( F_z^{(1)} + \Phi_y^{(1)} \right) \right), \quad (24)$$

$$v^s \sim v^{s0} + \varepsilon v^{s1} = \Phi_x^{(0)} - \varepsilon \left( G_z^{(1)} - \Phi_z^{(1)} \right).$$

## 2.2. Horizontal Advection

The horizontal winds (24) are used to advect the surface potential temperature  $\theta^s$  in (7). The artificial dissipation operator is given by the eighth-order horizontal hyper viscosity (4). This representation for dissipation has little connection to the real physics in primitive equations, and is used in numerical experiments to control the buildup of variability on small grid-scales. Applying Fourier and sine transforms consequently ( $\mathcal{F}$ ) to (4) gives the spectral form of the governing equation

$$\frac{\partial \hat{\theta}^s}{\partial t} = \mathcal{F} \left[ -u^s \frac{\partial \hat{\theta}^s}{\partial x} - v^s \frac{\partial \hat{\theta}^s}{\partial y} \right] - \nu \left( k^2 + l^2 \right)^4 \hat{\theta}^s. \quad (25)$$

This equation then is forced randomly at high wavelengths in the spectral space, and direct numerical simulations are performed with a resolution of  $512 \times 256$  horizontal wave numbers. Temporal discretization is realized by the second-order predictor-corrector finite-difference scheme.

## 3. Numerical Simulations

To compare the properties of forced  $\beta$ - $sQG^{+1}$  turbulence with the freely evolving regime we ran both simulations, with and without stochastic forcing. The forcing term is introduced as a random field in the spectral space supplied at high wavelength. Each of the simulations starts from the same random initial conditions and the time step is  $\tau = 0.01$  in non-dimensional time units. One non-dimensional time unit is approximately equal to 12 hour. The simulations are made for an area that has a channel geometry with dimensions  $10\pi$  in the zonal and  $6\pi$  in the meridional directions that correspond to approximately 31,000 km length and 18,000 km width. Note that non-dimensional length unit is about 1000 km. The parameters were chosen to represent the mid-latitude atmospheric dynamics

◇ Rossby number  $\varepsilon = 0.2$

◇ Meridional vorticity gradient  $\beta = 2$

◇ Vertical shear  $\Lambda = 0$

where the vertical shear was particularly chosen zero in order to avoid its influence. The evolution of the freely evolving  $\beta$ - $sQG^{+1}$  surface potential temperature from random initial conditions shown in **Figure 1**. As it was initially found in [5] inclusion of  $\beta$ -effect in the higher-order nonlinear dynamics added a wave term that competes with inertia on large-scales and produced high meridional asymmetries in the eddies deformation radius. This novel feature was added to the standard for the  $\beta$ -plane turbulence zonal asymmetry, *i.e.* formed zonal jets. The zonal jet formation is shown in **Figure 2**.

The evolution of the forced  $\beta$ - $sQG^{+1}$  turbulence form random initial conditions is shown in **Figure 3**. The simulations in the forced regime exhibit not only anisotropy in the eddies spatial and time scales, but also in their orientation. In addition to the established wave-like motion, after some time there is an evident tendency of the flow to stretch vortices in preferred direction. As it can be seen from the direct numerical simulations the cold anomalies are always stretched in the north-eastward direction, while the warm anomalies are stretched in the north-westward direction.

However to catch exactly directions of the formed vortices we used one point correlation method. The correlation function represents a statistical process, and as a statistical quantity should be calculated over a long interval of time. The correlation is large and positive if the elements tend to be in a phase, *i.e.* positive picks tend to occur together. The correlation is strongly negative, if the elements are in the opposite phase, *i.e.* the peaks in one occur when valleys are attained in the other. Finally, the correlation function vanishes if the two variables are 90 degrees out-of-phase, *i.e.* one is passing through zero at the peak or valley of the other.

For a fixed element with coordinates (40,80) we calculated its correlation with the others elements, and correlation function contour lines are shown in **Figure 4**. The left-hand side panel of **Figure 4** shows positive correlation of the reference point (40,80) with the other elements, while the right-hand side panel represents the negative correlation with the reference point. Those directions coincide with the observed north-western elongation of the worm anomalies and the north-eastern elongation of the cold anomalies in the the potential temperature evolution (3).

To see the persistence of the zonal flow we calculated time sequence of the zonal mean of the potential temperature at each latitude and the contour map is given in **Figure 5**. This map illustrates that zonal jets are indeed formed and in addition there is a meridional (northern/southern) meandering of the formed jets. This novel property is in accordance with the well known from the ob-

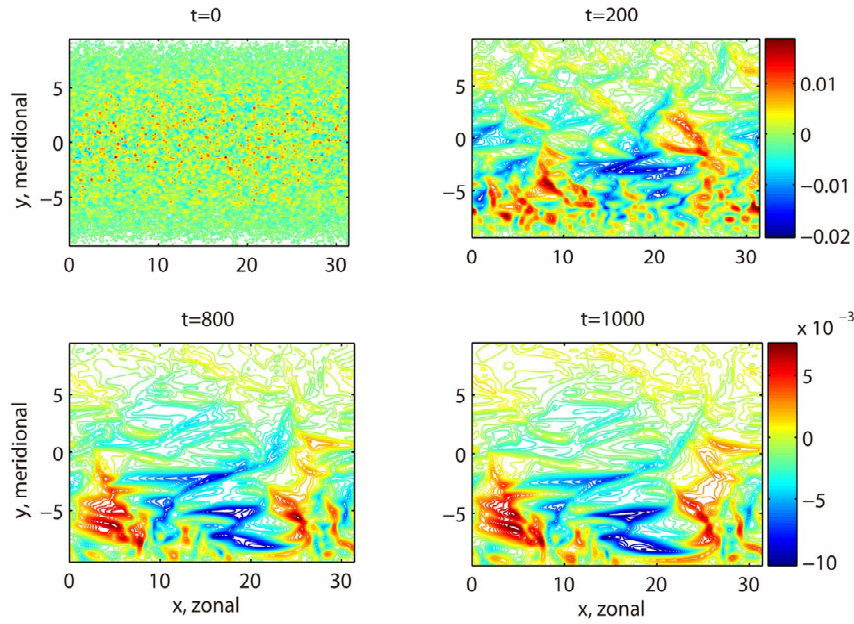


**Figure 1.** Surface potential temperature evolution from random initial conditions of the freely evolving  $\beta - sQG^{+1}$  turbulence. Instantaneous contour lines are given at the initial moment  $t = 0$ , at the moment  $t = 200$ ,  $t = 800$ , and  $t = 1000$  non-dimensional time. 1 time unit  $\approx 12$  hours. Length scale is given in non-dimensional units with 1 length unit  $\approx 1000$  km.

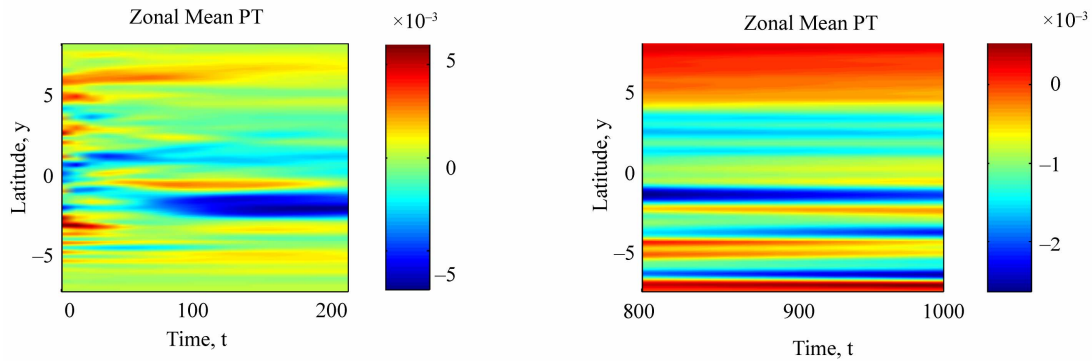


**Figure 2.** Contours of the zonal mean of the freely evolving potential temperature as a function of time and latitude showing the jets formation. Time and latitude are given in non-dimensional units.

servational studies jet-meandering in the large-scale mid-latitudes.

### 4. Conclusions

Forced  $\beta$ -plane turbulence stabilized by large scale friction tends to develop anisotropy and accumulate energy in zonal (or near zonal) modes. In this study we showed something more, namely that forced  $\beta$ -plane turbulence develops not only zonal, but also meridional asymmetry. Direct numerical simulations presented here illustrate the meridional meandering of the formed zonal jets. The inclusion of the meridional variation in the Coriolis parameter ( so called  $\beta$ -effect) into the weakly nonlinear dynamics and the presence of some stochastic

forcing resulted in a theoretical model that captures both, meridional asymmetries in the deformation radius and orientation of the large-scale coherent structure formations. A very intriguing novel feature of the forced  $\beta - sQG^{+1}$  model was found, namely the warm anomalies are always elongated in the north-western direction while the cold anomalies are always oriented to the north-east. The performed numerical simulations have shown that the combined presence of the  $\beta$ -effect and stochastic forcing have important influence on the large-scale mid-latitude nonlinear atmospheric dynamics and may explain the meridional meandering of the jet-streams well known from the observational studies. The fact that  $\beta - sQG^{+1}$  numerical model was able to capture those novel meridional asymmetries in the large-

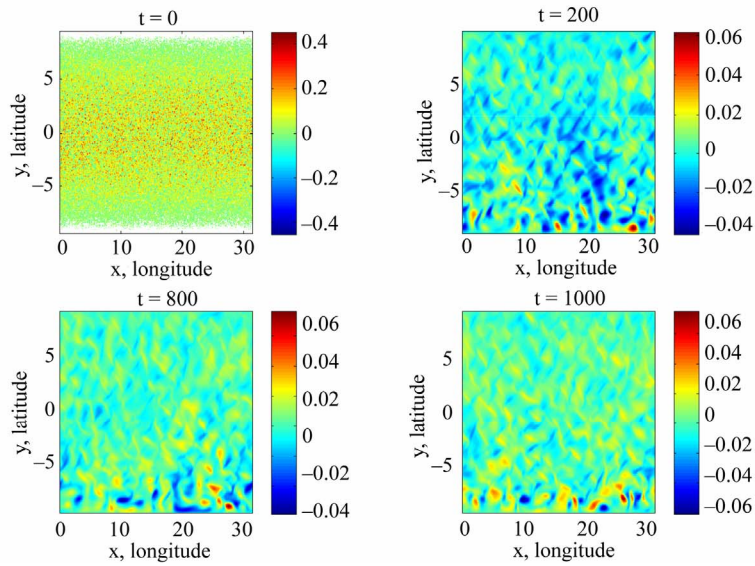


**Figure 3.** Surface potential temperature evolution of the forced  $\beta - sQG^{+1}$  turbulence from random initial conditions. Instantaneous contour lines are given at the initial moment  $t = 0$ , at the moment  $t = 200$ ,  $t = 800$ , and  $t = 1000$  non-dimensional time. 1 non-dimensional time unit  $\approx 12$  hours. Length scale is given in non-dimensional units with 1 length unit  $\approx 1000$  km.

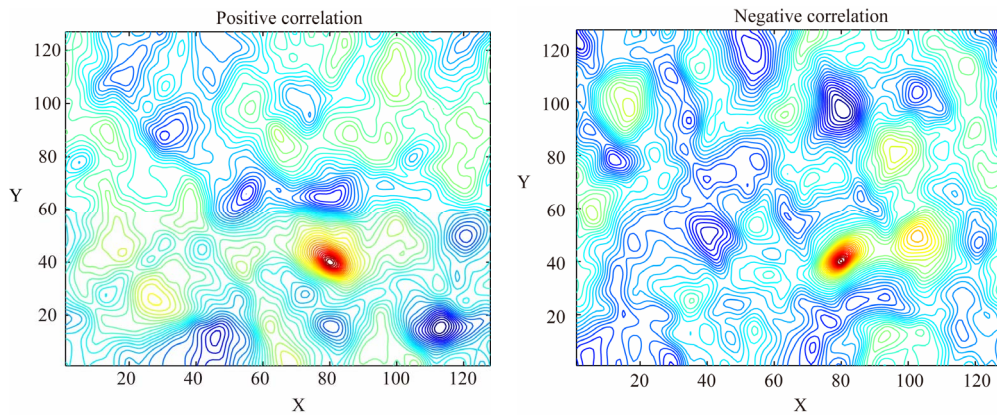


**Figure 4.** Correlation function contour lines for the element with coordinates (40,80) with respect to the positive elements (to the left), and with respect to the negative elements (to the right).

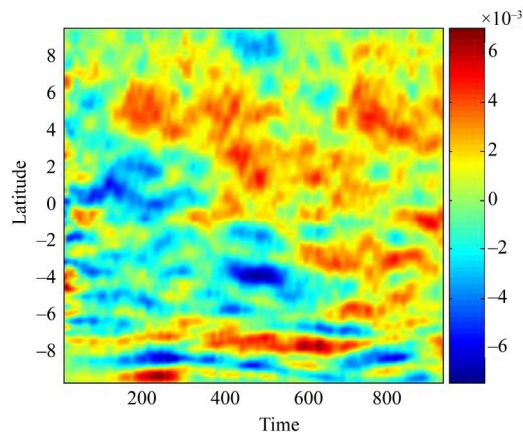


**Figure 5.** Contours of the zonal mean of the forced potential temperature as a function of time and latitude showing the meridional meandering of the formed jets. Time and latitude are given in non-dimensional units.

scale dynamics proved again the usefulness of this model as a tractable model for wave-turbulence interactions in a continuously stratified rotating flow.

## 5. Acknowledgements

This work was supported in part by a grant of computer time from the Department of Defence High Performance Computing Modernization Program at the Aeronautical Systems Center Major Shared Resource Center located at Wright-Paterson Air Force Base in Ohio.

## 6. References

- [1] M. Jukes, "Quasi-geostrophic Dynamics of the Tropopause," *Journal of the Atmospheric Sciences*, Vol. 51, No. 19, 1994, pp. 2756-2768. [doi:10.1175/1520-0469\(1994\)051<2756:QDOT>2.0.CO;2](https://doi.org/10.1175/1520-0469(1994)051<2756:QDOT>2.0.CO;2)
- [2] I. M. Held, R. T. Pierrehumbert, S. T. Garner and K. L. Swanson, "Surface Quasi-Geostrophic Dynamics," *Journal of Fluid Mechanics*, Vol. 282, 1995, pp. 1-20. [doi:10.1017/S0022112095000012](https://doi.org/10.1017/S0022112095000012)
- [3] G. J. Hakim, C. Snyder and D. J. Muraki, "A New Surface Model for Cyclone-Anticyclone Asymmetry," *Journal of the Atmospheric Sciences*, Vol. 59, No. 16, 2002, pp. 2404-2420.
- [4] P. B. Rhines, "Waves and Turbulence on a  $\beta$ -Plane," *Journal of Fluid Mechanics*, Vol. 69, No. 3, 1975, pp. 417-443. [doi:10.1017/S0022112075001504](https://doi.org/10.1017/S0022112075001504)
- [5] I. N. Panayotova, "A New Surface Model for  $\beta$ -Plane Turbulence," *Journal of the Atmospheric Sciences*, Vol. 64, No. 7, 2007, pp. 2717-2725. [doi:10.1175/JAS3970.1](https://doi.org/10.1175/JAS3970.1)
- [6] I. N. Panayotova, "Nonlinear Effects in the Extended Eady Model: Nonzero  $\beta$  but Zero Mean PV Gradient," *Dynamics of Atmospheres and Oceans*, Vol. 50, No. 1, 2010, pp. 93-111. [doi:10.1016/j.dynatmoce.2010.02.001](https://doi.org/10.1016/j.dynatmoce.2010.02.001)